Inorganic Chemistry

Article

pubs.acs.org/IC

Generation of Dihydrogen Molecule and Hydrosilylation of Carbon Dioxide Catalyzed by Zinc Hydride Complex: Theoretical Understanding and Prediction

Milind Madhusudan Deshmukh*[,†,‡] and Shigeyoshi Sakaki*[,†]

[†]Fukui Institute for Fundamental Chemistry, Kyoto University, Nishi-hiraki cho, Takano, Sakyo-ku, Kyoto 606-8103, Japan

[‡]Department of Chemistry, Dr. Harisingh Gour Central University, Madhya Pradesh, Sagar 470 003, India

Supporting Information

ABSTRACT: Generation of H_2 from methanol/water and hydrosilylation of CO_2 catalyzed by [tris(2-pyridylthio)methyl]zinc hydride [κ^3-Tptm]ZnH **1** were investigated with DFT and MP2 methods. The hydrosilylation of CO_2 occurs via the CO_2 insertion into the Zn−H bond of **1** followed by the metathesis of a Zn−(η^1-OCOH) bond with hydrosilane to yield silyl formate and regenerate **1**. The CO_2 insertion easily occurs, but the metathesis is difficult because of the formation of a very stable Zn−(η^2-O_2CH) species before the metathesis. The $\Delta G^{\circ\ddagger}$ value of the metathesis with triethoxysilane is much smaller than that with phenylsilane because electronegative methoxy groups stabilize the transition state bearing hypervalent Si center, which is consistent with the experimental result that triethoxysilane is used in the hydrosilylation of CO_2. It is theoretically predicted here that hydrosilane with two electronegative OEt groups or one to three F groups can be applied to this reaction. In the generation of H_2 from methanol/water by **1**, the first step is the metathesis of **1** with the O−H bond of methanol/water to produce [κ^3-Tptm]Zn(OMe)/[k^3-Tptm]Zn(OH) and dihydrogen molecule. The next step is the metathesis of the Zn−OMe/Zn−OH bond with hydrosilane to yield silyl ether and regenerate **1**. The first metathesis is rate-determining but the second one occurs with very small activation energy, indicating that various hydrosilanes can be applied to this reaction.

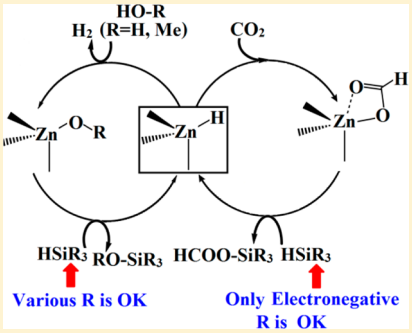

INTRODUCTION

The limited resources of fossil fuels and the environmental problems induced by their use demand that we look for alternative energy resources. Such resources must be abundant, easy to use, and induce less or no hazardous impact on the environment. One promising candidate is dihydrogen molecule, which can efficiently produce energy without any hazardous byproduct.[1] In this regard, various attempts have been made to produce hydrogen gas from biomasses such as ethanol and methanol.[2] Unfortunately, however, the physical property of dihydrogen molecule makes it difficult to handle, store, and transport hydrogen gas, as is well-known. Though many efforts have been made to safely store hydrogen gas,[3−5] drawbacks are still pointed out.[6] To avoid the difficulty of storage, a lot of efforts have been made for on-demand generation of hydrogen gas. For instance, many substrates such as ammonia borane and related compounds,[7] organic heterocycles,[8] formic acid,[9] alcohol,[2,10] and organic silanes[11] have been applied to the reaction. Among them, many organometallic chemists are interested in hydrolysis and alcoholysis of the Si−H bond of organic silanes,[11−16] because many transition metal complexes are expected to be applied to these reactions. Though these reactions are simple and thermodynamically favorable and also various organic silanes are available nowadays, these reactions are kinetically slow and need a catalyst consisting of precious metal.[17−20]

Another serious environmental problem arising from the use of fossil fuels is the global warming caused by carbon dioxide (CO_2), which is a byproduct of combustion of fossil fuels. Removal of CO_2 from the environment is primarily important in the scientific community over the past two decades. One of the desirable solutions is to convert CO_2 into useful chemicals, because it is an abundant renewable carbon source. Transition metal complexes act as an effective catalyst for CO_2 fixation reaction, as is well-known.[21] Among various transition-metal-catalyzed CO_2 fixation reactions with such reactive substrates as epoxides, alcohols, amines, and alkynes, the most straightforward CO_2 fixation is the hydrogenation of CO_2 to formic acid.[21−23] However, this reaction generally requires the consumption of base to stabilize formic acid, because formic acid is thermodynamically less stable than the sum of CO_2 and H_2. Alternatively, the hydrosilylation of CO_2 with hydrosilane to silyl formate is thermodynamically favorable because of the formation of the strong Si−O bond. Moreover, silyl formate can be converted to formic acid,[22] formamide,[23] and silicon-based polymeric materials,[24] indicating that the hydrosilylation of CO_2 is a promising route for the CO_2 fixation. However, expensive catalysts such as rhodium,[23] ruthenium,[25] and iridium[26] complexes were employed. One exception is a copper

Received: May 7, 2014
Published: July 30, 2014

   dx.doi.org/10.1021/ic501058j | Inorg. Chem. 2014, 53, 8485−8493

catalyst reported by Motokura et al.[23a] Moreover, most of them require high CO_2 pressure to produce high yield of the product.

Considering these circumstances found in the CO_2 fixation and on-demand generation of hydrogen gas, we need an efficient catalyst with abundant metal. A recently reported multifunctional catalyst of a [tris(2-pyridylthio)methyl]zinc hydride, [κ^3-Tptm]ZnH **1**,[27] solves these problems, because abundant and cheap zinc metal is used in this efficient catalyst. Interestingly, **1** is capable of achieving both the rapid on-demand generation of dihydrogen molecule and the hydrosilylations of aldehydes, ketones, and CO_2 (Scheme 1). Despite these interesting catalytic reactions by **1**, the reaction mechanism, rate-determining step, and characteristic features of the transition state are unclear. Also it was reported that triethoxysilane was used in the hydrosilylations of CO_2 but phenylsilane was in the on-demand generation of dihydrogen molecule from alcohol/water. Theoretical knowledge of how to employ hydrosilane in these reactions is indispensible for achieving further development of this catalytic system.

Scheme 1. Experimentally Reported Catalytic Cycle for H_2 Generation with Methanol/Water (Left) and Hydrosilylation of CO_2 (Right) Catalyzed by [κ^3-Tptm]ZnH 1

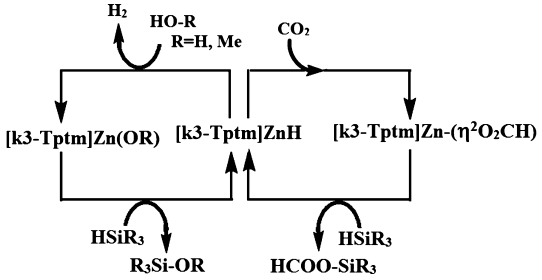

In this work, we theoretically investigated two catalytic reactions by **1**, the hydrosilylation of CO_2 and the generation of dihydrogen molecule from methanol/water and silane. Our purposes here are to clarify the reaction mechanisms of these two catalytic reactions, uncover characteristic features of the electronic process of each elementary step, and elucidate the reason why triethoxysilane was used in the hydrosilylation of CO_2 but phenylsilane was employed in the on-demand generation of dihydrogen molecule from alcohol/water. Also, we wish to propose a theoretical prediction of what hydrosilane can be applied to these reactions.

COMPUTATIONAL DETAILS

Geometries of all the species studied in this work were optimized by the DFT method with the B3PW91 functional.[28,29] Two kinds of basis set systems, BS-I and BS-II, were used in this work. In BS-I, 6-31G(d) basis sets[30] were employed for all atoms. This BS-I was employed for the geometry optimization. The optimized geometries are close to the experimentally reported X-ray structures;[27] see Table S1 in the Supporting Information. Vibration frequencies of each optimized species were calculated to check whether it is an equilibrium structure or a transition state. The better basis set system BS-II was used for evaluating changes in energy and population, where the DFT/BS-I-optimized geometries were employed. In BS-II, a (311111/22111/411) basis set was employed for Zn, where its core electrons were replaced by the Stuttgart−Dresden−Bonn (SDD) effective core potentials (ECPs).[31] 6-311G(d) basis sets were used for H, C, N, O, Si, and S atoms, where one set of p-polarization functions was added to the hydride (H) ligand of the catalyst **1**, the H of hydrosilane, and the H of hydroxyl group in methanol/water and one set of diffuse functions was added to C and O atoms of CO_2, −OMe, and −OCOH groups.[32] The MP2/BS-II method was employed for evaluating the energy changes because this method provides the similar energy changes to the CCSD(T)-calculated values; see page S4 and Figures S1 to S4 in the Supporting Information. The Gibbs energy was used for the discussion, where the translational entropy was corrected with the method developed by Whitesides et al.[33] The natural bond orbital

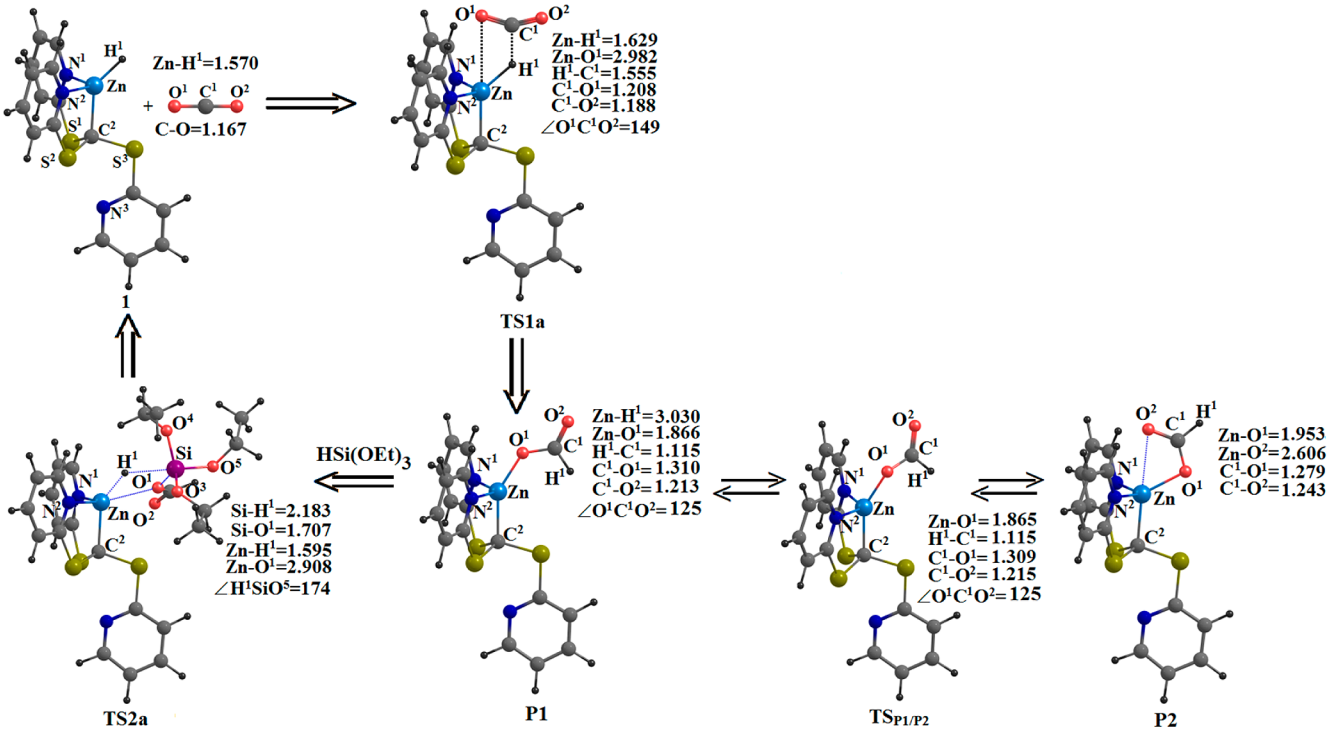

Figure 1. Geometrical changes in the reaction of CO_2 with a [κ^3-Tptm]Zn−H **1**. Bond lengths are in angstroms and bond angles in degrees.

dx.doi.org/10.1021/ic501058j | Inorg. Chem. 2014, 53, 8485−8493

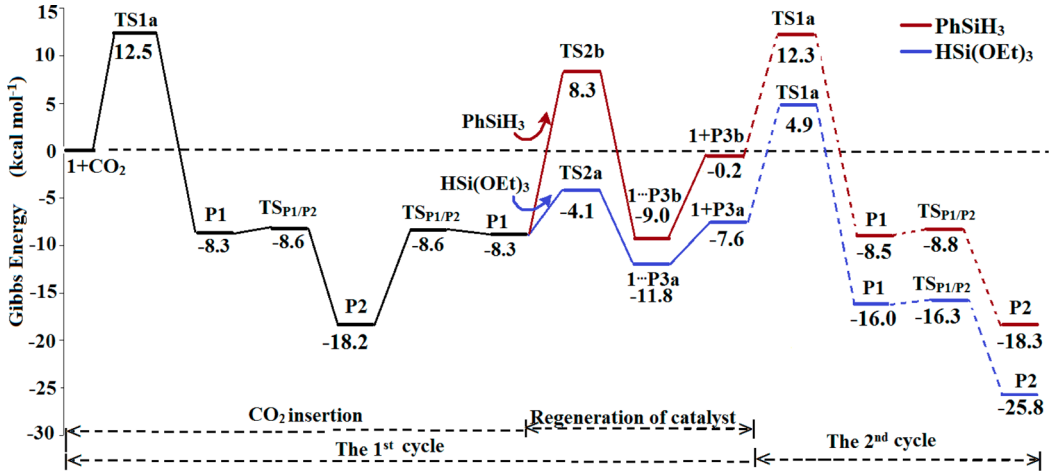

Figure 2. Gibbs energy changes in the hydrosilylation of CO_2 catalyzed by [κ^3-Tptm]ZnH **1**. See Figure 1 for geometries. The potential energies were calculated at the MP2 level. The thermal energy and the entropy were calculated at the DFT level.

(NBO) population analysis was carried out with the electron density at the MP2 level. All calculations were performed with the Gaussian09 program package.[34]

RESULTS AND DISCUSSION

The Catalytic Cycle of the Hydrosilylation of CO_2. The first step of the catalytic cycle is the CO_2 insertion into the Zn−H bond of [κ^3-Tptm]ZnH **1**, which occurs through a transition state **TS1a** to form an η^1-coordinated formate intermediate [κ^3-Tptm]Zn(η^1-OCOH) **P1**, as shown in Figure 1. In **TS1a**, the C and O atoms of CO_2 are approaching the hydride and Zn of **1**, respectively, from the top side; see Figure 1. The Zn−H and C−O bonds become somewhat longer and the O^1−C^1−O^2 angle becomes considerably smaller in **TS1a** than in **1**. The Zn−O^1 and H^1−C^1 distances are, however, still considerably large, suggesting that the Zn−O^1 and H^1−C^1 bonds are not completely formed yet in **TS1a**. The Gibbs activation energy ($\Delta G^{\circ\ddagger}$) and reaction energy (ΔG°) are 12.5 kcal/mol and −8.3 kcal/mol, respectively, as shown in Figure 2, where a negative ΔG° value represents exergonic reaction. These values indicate that CO_2 is easily inserted into the Zn−H bond.

P1 isomerizes to a more stable η^2-coordinated formate complex **P2** through a transition state $\mathbf{TS_{P1/P2}}$. The optimized geometry of **P2** agrees with the experimentally reported X-ray structure;[27] see Table S1 in the Supporting Information. In the transition state, only the Zn−O^1−C^2−H^1 dihedral angle considerably increases. Because the dihedral angle easily changes without a large energy change in general, the $\Delta G^{\circ\ddagger}$ is small (0.3 kcal/mol).[35] The ΔG° is very negative (−9.9 kcal/mol relative to **P1**) because **P2** is stabilized by two Zn−O bonding interactions. In **P2**, the Zn−O^2 bond is considerably longer than the Zn−O^1 bond. This is because the alkyl group with large trans influence exists at the position trans to the Zn−O^2 bond. Because **P2** is very stable, it is considered to be a resting state, as discussed in the experimental work.[27]

Also, **P2** can be directly formed starting from **1** through a transition state **TS1b**, in which CO_2 approaches **1** from the side direction; see Figure S5A in the Supporting Information. The $\Delta G^{\circ\ddagger}$ value (19.3 kcal/mol) is much larger than in the reaction via **TS1a**. Hence, this reaction course is ruled out. We will not discuss further this pathway.

The next step is the reaction between **P2** and hydrosilane. However, the structure of **P2** is unfavorable for this reaction because the five-coordinated Zn center in **P2** does not have enough space for an incoming hydrosilane. It is likely that the next reaction with hydrosilane starts from **P1** because **P1** has an unoccupied coordination site; the IRC calculation certified it. This means that **P2** isomerizes back to **P1** and then **P1** reacts with $HSi(OEt)_3$ through a transition state **TS2a** to afford a silyl formate $HCOOSi(OEt)_3$ **P3a** and regenerate **1**; see Figure 1. In **TS2a**, the Zn and O^1 atoms of the Zn−(η^1-OCOH) moiety approach the H^1 and Si atoms of $HSi(OEt)_3$, respectively; see Figure 1. It should be noted that the Si atom has a distorted trigonal bipyramidal structure. This is similar to the geometry of the hypervalent Si species. In **TS2a**, three OEt groups are bound with the Si center, which is favorable for stabilizing **TS2a**; remember that electronegative groups are found in general in the hypervalent Si compounds. The $\Delta G^{\circ\ddagger}$ is 14.1 kcal/mol and the ΔG° is 6.4 kcal/mol relative to **P2**, indicating that this process is not difficult. The somewhat large $\Delta G^{\circ\ddagger}$ value calculated here is consistent with the rather high reaction temperature (100 °C).[27]

We also investigated the metathesis between **P1** and $PhSiH_3$ to compare reactivity between $PhSiH_3$ and $HSi(OEt)_3$. The geometry changes are similar between $HSi(OEt)_3$ and $PhSiH_3$; see Figure S5B in the Supporting Information. On the other hand, the $\Delta G^{\circ\ddagger}$ (26.5 kcal/mol) is considerably large and the ΔG° (9.2 kcal/mol) is considerably more positive in the metathesis with $PhSiH_3$, indicating that this metathesis is difficult; see Figure 2. In a transition state **TS2b**, the Si atom has a hypervalent trigonal bipyramidal structure too. However, this structure is not favorable for the hypervalent Si species, because no electronegative group is bound with the Si center. Actually, the H^1SiH^2 angle (165°) of **TS2b** is smaller than the H^1SiO^5 angle (171°) of **TS2a**, indicating that **TS2a** is close to the typical hypervalent structure but **TS2b** somewhat deviates; remember that those angles are 180° in the typical trigonal bipyramidal structure. These geometrical features relate to the higher activation energy for **TS2b** than for **TS2a**, which will be discussed below in more detail.

As shown in Figure 2, the final product, **1** + silyl formate **P3**, is more unstable than the most stable intermediate **P2** in both cases of $HSi(OEt)_3$ and $PhSiH_3$. However, the exergonic nature of subsequent steps can compensate for this. To verify that, we examined the second cycle. As shown in Figure 2, the catalytic reaction must proceed from **P2** in the first cycle to **P2** in the

dx.doi.org/10.1021/ic501058j | Inorg. Chem. 2014, 53, 8485−8493

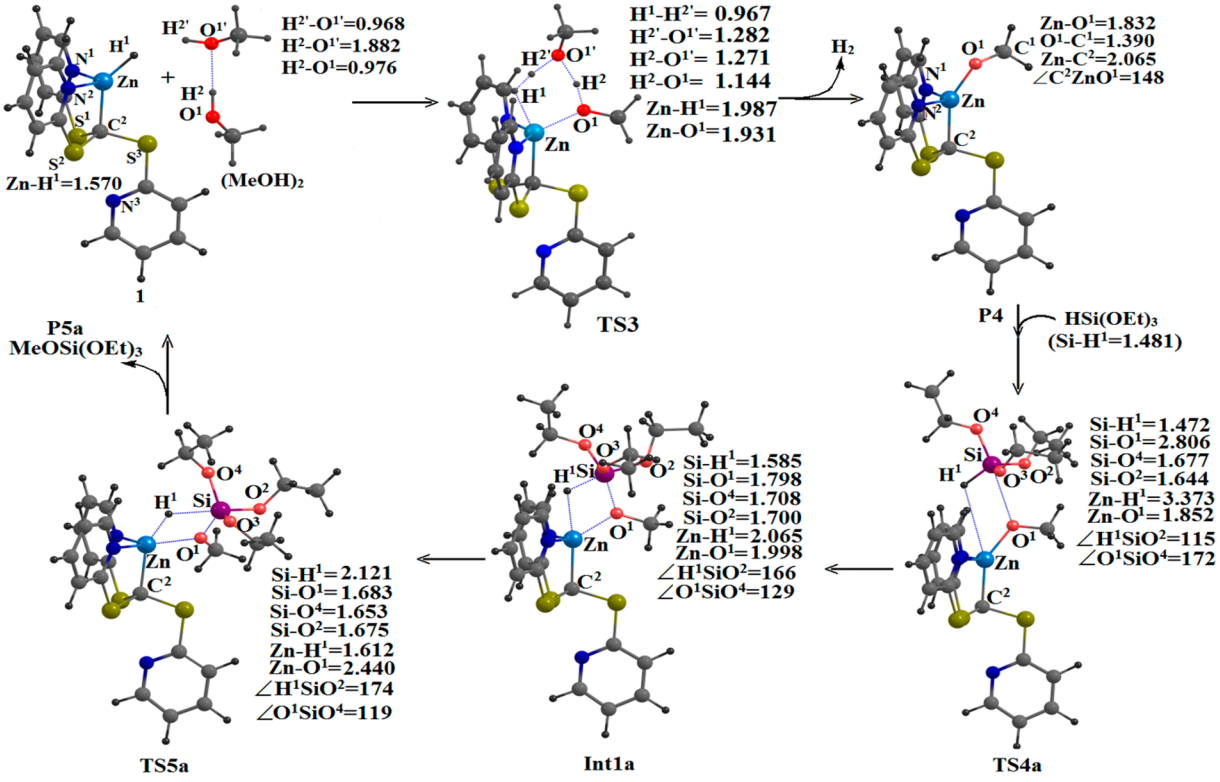

Figure 3. Geometry changes in the generation of dihydrogen molecule from methanol catalyzed by [κ^3-Tptm]ZnH **1**. Bond lengths are in angstroms and bond angles in degrees.

next cycle to complete the catalytic cycle. The most stable species is **P2**, and the highest transition state is **TS1a** in both hydrosilanes. Hence, the $\Delta G^{\circ\ddagger}$ value to complete a catalytic cycle corresponds to the energy difference between **P2** in the first cycle and **TS1a** in the second cycle. As shown in Figure 2, the $\Delta G^{\circ\ddagger}$ value is 23.1 kcal mol^{-1} in the case of $HSi(OEt)_3$ but 30.5 kcal mol^{-1} in the case of $PhSiH_3$. These results are consistent with the experimental fact that not $PhSiH_3$ but $HSi(OEt)_3$ was used in this reaction.

The Catalytic Cycle of the Generation of H_2 from Methanol/Water. In the H_2 generation reaction, **1** reacts with methanol to afford a dihydrogen molecule and a zinc methoxide complex [κ^3-Tptm]Zn(OMe) **P4** through a transition state **TS3**, as shown in Figure 3. As moving to **TS3** from the reactants, the Zn−H^1 bond length considerably increases but the O^1−H^2 bond length of methanol moderately increases. The Zn−O^1 bond is only 10% longer in **TS3** than in **P4**, while the H^1−H^2 bond length is considerably longer in **TS3** than in free dihydrogen molecule (the optimized value is 0.741 Å). These geometrical features indicate that the Zn−H^1 bond breaking and Zn−O^1 bond formation occur prior to the O^1−H^2 bond breaking and the H^1−H^2 bond formation, suggesting that the approach of MeOH to Zn and the O−H bond elongation are the origin of the activation energy. It should be noted that two MeOH molecules participate in the reaction to form a proton chain with the six-member ring in **TS3**. The $\Delta G^{\circ\ddagger}$ and ΔG° values are 10.6 kcal/mol and −8.1 kcal/mol,[36] respectively, indicating that this step is not difficult; see Figure 4. If only one MeOH participates in the reaction, the ΔG° value is 17.1 kcal/mol; see Figure S8 in the Supporting Information for geometry changes.[37]

In the next step, **P4** reacts with hydrosilane to reproduce the catalyst **1**. As seen in Figure 3, the Si and H atoms of

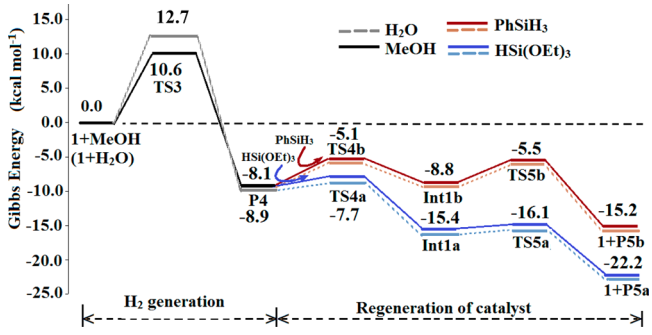

Figure 4. Gibbs energy changes in the generation of H_2 catalyzed by **1**. See Figure 3 for geometries. The potential energies were calculated at the MP2 level. The thermal energy and the entropy were calculated at the DFT level.

$HSi(OEt)_3$ approach the O^1 and Zn atoms of **P4**, respectively, to afford an intermediate **Int1a** through a transition state **TS4a**. In **TS4a**, the Si−H^1 bond is elongated a little and the Zn−H^1 and Si−O^1 distances are still very large. These geometrical features suggest that **TS4a** is reactant-like in which the Zn−H^1 and Si−O^1 bonds are not formed at all. The Si center has a distorted trigonal bipyramidal structure, in which the Si−O^1 distance is considerably longer than the Si−O^4 distance; in other words, a pure hypervalent Si species is not formed in **TS4a**. In **Int1a**, the Si−O^1 distance considerably decreases and becomes similar to the Si−O^2 distance. The H^{1}SiO^2 angle is 166°, which is close to 180°. These features clearly indicate that the Si center takes a five-coordinate trigonal bipyramidal structure in which the H^1 and O^2 atoms exist on the axial positions. This is a typical hypervalent Si structure. The Zn−H^1 distance considerably decreases in **Int1a**, but it is still

dx.doi.org/10.1021/ic501058j | Inorg. Chem. 2014, 53, 8485−8493

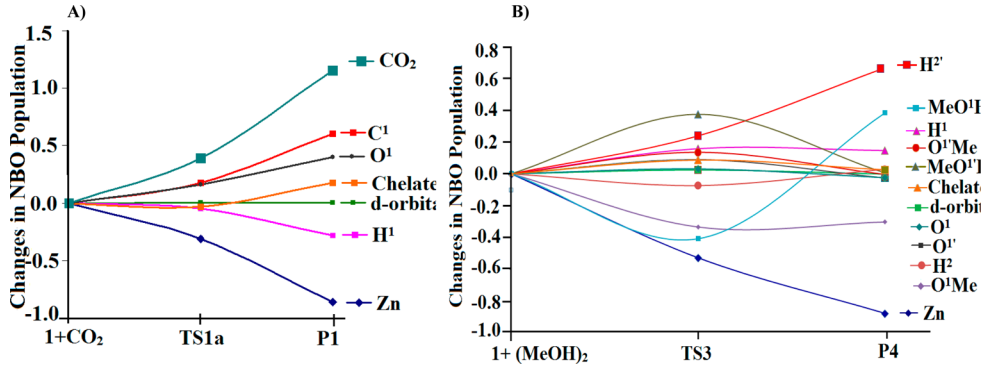

Figure 5. Changes in the NBO populations in (A) the CO_2 insertion into the Zn−H bond of **1** and (B) the metathesis of the Zn−H bond of **1** with methanol.

considerably larger than in **1**, indicating that the Zn−H^1 bond formation is not completed yet. The $\Delta G^{\circ\ddagger}$ value is very small and ΔG° is −6.5 kcal/mol, indicating that this step occurs very easily (Figure 4).

Int1a is converted to the catalyst **1** with the release of triethoxymethoxysilane through a transition state **TS5a**; see Figure 3. In **TS5a**, the Si−H^1 and Zn−O^1 bonds become considerably longer and the Zn−H^1 and the Si−O^1 distances become substantially shorter, indicating that the Zn−H^1 and Si−O^1 bonds are almost formed and the Si−H^1 and Zn−O^1 bonds are almost broken. The $\Delta G^{\circ\ddagger}$ value is nearly zero and the ΔG° is −6.8 kcal/mol, indicating that this step occurs very easily (Figure 4).[38]

The reaction of **P4** with $PhSiH_3$ occurs via **TS4b**, **Int1b**, and **TS5b** to regenerate **1**. The geometry changes are similar to those of the reaction with $HSi(OEt)_3$; see Figure S6 and page S14 in the Supporting Information. One important difference is found between **Int1a** and **Int1b**: in **Int1b**, the Si center has a hypervalent trigonal bipyramidal structure in which two H atoms exist on the axial positions but the Ph group exists on the equatorial position. This geometry is not favorable for the hypervalent species, because no electronegative group is bound with the Si center. As a result, **Int1b** is less stable than **Int1a**, as shown in Figure 4. Also, $(MeO)SiPhH_2$ **P5b** is less stable than $(MeO)Si(OEt)_3$ **P5a**. The $\Delta G^{\circ\ddagger}$ value is larger and the ΔG° is less negative in the reaction with $PhSiH_3$ than with $HSi(OEt)_3$. However, the $\Delta G^{\circ\ddagger}$ value is still small enough and the total ΔG° is negative enough, indicating that the reaction easily occurs even in the case of $PhSiH_3$.

Based on these energy changes, it should be concluded that the generation of dihydrogen molecule is rate-determining but the metathesis of the Zn−OMe bond with hydrosilane occurs very easily. These results indicate that various hydrosilanes including less reactive $PhSiH_3$ can be applied to the generation of H_2.

We investigated the on-demand production of dihydrogen molecule from water, but we wish to skip the discussion of the geometry changes, because the geometry changes are similar to those of the reaction with methanol; see Figures S7A and S7B in the Supporting Information for the geometry changes. The energy changes are similar to those of the reaction with MeOH, as shown in Figure 4.

Electronic Processes in the CO_2 Insertion into the Zn−H Bond of 1 and the Metathesis of the Zn−H Bond with Methanol/Water. In the CO_2 insertion going from **1** to **P1**, the Zn atomic population substantially decreases; see Figure 5A and also Table S5 in the Supporting Information for details. The 4s and 4p orbital populations of Zn substantially decrease, while the 3d orbital population of Zn changes little; see Table S5 in the Supporting Information. This is because Zn(II) has a stable $3d^{10}$ electron configuration. The H^1 atomic population only marginally decreases when going from **1** to **TS1a** but considerably when going from **TS1a** to **P1**. This is consistent with the moderate elongation of the Zn−H bond in **TS1a** but the considerable elongation in **P1**. In **TS1a**, the C^1 and O^1 atomic populations increase to a similar extent, while the Zn atomic population decreases much more than the H^1 atomic population. These changes suggest that the polarization of the Zn−O^1 bond occurs so as to decrease the Zn atomic population and increase the H^1 atomic population; note that if the polarization does not occur and only the CT occurs from the Zn to O^1, the O^1 atomic population increases more than the H^1 population. It should be noted that the electron population of the CO_2 moiety considerably increases and its increase is similar to the sum of the decreases in the Zn and H^1 atomic populations. Based on these results, it is concluded that charge transfer (CT) occurs from the Zn−H^1 moiety to the CO_2 moiety concomitantly with the polarization of the Zn−H^1 bond, as shown in the left side of Scheme 2. This significantly

Scheme 2. Similarity in Population Changes between the CO_2 Insertion into the Zn−H Bond (Left Side) and the Metathesis of the Zn−H with MeOH (Right Side)

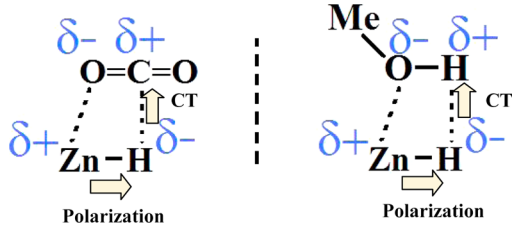

large CT is one of the important characteristic features of the CO_2 insertion reaction, as was reported previously.[39] The electron population of the k^3-Tptm ligand changes little, suggesting that the κ^3-Tptm ligand participates in the population changes little.

In the metathesis of the H_2 generation reaction going from **1** to **P4**, the Zn atomic population substantially decreases too; see Figure 5B and Table S6 in the Supporting Information. The 3d orbital population of Zn changes little, but the 4s and 4p orbital populations of Zn considerably decrease. These are essentially the same as the CO_2 insertion into the Zn−H bond of **1**.

dx.doi.org/10.1021/ic501058j | Inorg. Chem. 2014, 53, 8485−8493

However, the H^1 atomic population somewhat increases when going from **1** to **TS3** but then moderately decreases when going from **TS3** to **P4** unlike in the CO_2 insertion. The H^2 atomic population of MeOH somewhat increases in **TS3** and then substantially increases when going from **TS3** to **P4**. The electron population of the O^1Me moiety does not change very much because it has already enough electron population in MeOH. These results are reasonably understood, as follows: (i) The elongation of the Zn−H^1 bond decreases the donation from the H^1 (hydride) to the Zn, which leads to an increase in the H^1 atomic population and a decrease in the Zn atomic population. This corresponds to the polarization of the Zn−H bond. Simultaneously, (ii) the CT occurs from the H^1 to the H^2 because the H^1 obtains more electron density from the Zn center and the H^2 is originally proton-like (electron-deficient) in MeOH, as shown in the right side of Scheme 2.

Though the CO_2 insertion into the Zn−H bond is completely different from the metathesis of the Zn−H with methanol, the similar population changes are found interesting. The similarity in population changes can be easily understood by Scheme 2. In the CO_2 insertion, the negatively charged O atom approaches the Zn and the positively charged C atom approaches the H (hydride). In the metathesis, the negatively charge OMe group approaches the Zn and the positively charged H of MeOH approaches the H (hydride). Hence, the population changes are similar between these two reactions. It is noted that the Zn atom plays an important role in supplying electron population to the substrate in both the CO_2 insertion and the metathesis with methanol.

Electronic Processes in the Metatheses of [κ^3-Tptm]-Zn(η^1-OCOH) P1 and [κ^3-Tptm]Zn(OMe) P4 with Hydrosilane. In the reaction of **P1** with $HSi(OEt)_3$, the most important feature is that the Si moiety becomes the hypervalent species in **TS2a**, as was seen in Figure 1. Consistent with the formation of the hypervalent Si species, the Si atomic population substantially decreases, because the Si center is positively charged in the hypervalent Si species in general; see Figure S9 and the discussion on page S20 in the Supporting Information for details of population changes.

In **TS2b** of the reaction of **P1** with $PhSiH_3$, the Si center has a more distorted trigonal bipyramidal structure than in **TS2a**, indicating that the hypervalent character in **TS2b** is less than in **TS2a**. Consistent with this difference, the electron population changes are somewhat different from those in the reaction with $HSi(OEt)_3$. When going from **P1** to **TS2b**/**TS2a**, the Si atomic population decreases less in the reaction with $PhSiH_3$ than in that with $HSi(OEt)_3$; see Figure S9 in the Supporting Information. This difference suggests that the electronic structure of the reaction system changes less easily in the case of $PhSiH_3$ than in the case of $HSi(OEt)_3$, which is consistent with the larger $\Delta G^{o\ddagger}$ value of the reaction with $PhSiH_3$ than with $HSi(OEt)_3$. Hence, it is of considerable importance to elucidate the reason why $HSi(OEt)_3$ leads to the formation of larger hypervalency in **TS2a** than does $PhSiH_3$ in **TS2b**.

To understand difference in reactivity between $HSi(OEt)_3$ and $PhSiH_3$, we inspected the transition states **TS2a** and **TS2b** in the reactions of **P1** with $HSi(OEt)_3$ and $PhSiH_3$, respectively. In **TS2a**, three electronegative OEt groups are bound with the Si center. In **TS2b**, on the other hand, no electronegative group is bound with the Si center. Because the hypervalent species wants to have the electronegative group(s), **TS2a** is more stable than **TS2b**. This is also the reason why $HSi(OEt)_3$ much more easily induces the electron population changes than does $PhSiH_3$. Based on these results, it is concluded that the larger stability of the hypervalent silicon species in **TS2a** is responsible for the larger reactivity of $HSi(OEt)_3$ than $PhSiH_3$.

To evaluate how much the stability of the hypervalent species depends on the substituents on the Si center in **TS2a** and **TS2b**, the formation of hypervalent silicon species was investigated, as shown in Scheme 3. In this evaluation, the

Scheme 3. Formation Reaction of Hypervalent Si Species

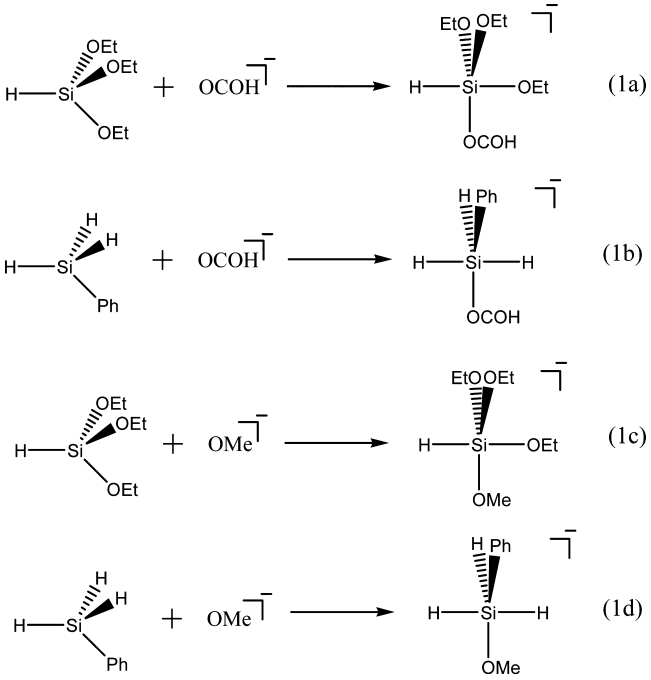

axial and equatorial substituents were taken to be the same as those in **TS2a** and **TS2b** and then the geometries of the corresponding hypervalent silicon species were optimized at the MP2/6-31G(d,p) level;[40] see Figure S10 in the Supporting Information for optimized geometries. As seen in Table 1, the formation of a hypervalent silicon species $[HSi(OEt)_3(OCOH)]^-$ from $HSi(OEt)_3$ provides a much larger stabilization energy (ΔE_{st}) than the formation of $[PhSiH_3(OCOH)]^-$ from $PhSiH_3$; see also eqs 1a and 1b in Scheme 3. This difference (about 15 kcal mol^{-1}) in ΔE_{st} is not very different from that in the $\Delta G^{o\ddagger}$ value between **TS2a** and **TS2b**.

All these computational results indicate that the hypervalent silicon species are more stable in **TS2a** than in **TS2b**, and hence **TS2a** is more stable than **TS2b**. The higher stability of the hypervalent silicon species in **TS2a** than in **TS2b** arises from the presence of three electronegative OEt groups in $HSi(OEt)_3$ and the absence of such electronegative group in $PhSiH_3$.

On the basis of the above results, it should be concluded that $HSi(OEt)_3$ is more favorable for the reactions with **P2** than $PhSiH_3$. Hence, only reactive $HSi(OEt)_3$ can be applied to the hydrosilylation of CO_2 because the $\Delta G^{o\ddagger}$ value is intrinsically large in the reaction of **P2** with hydrosilane, which is a rate-determining step. On the other hand, less reactive $PhSiH_3$ can be used in the H_2 generation reaction because the $\Delta G^{o\ddagger}$ value is intrinsically small in the reaction of **P4** with hydrosilane, which is not a rate-determining step.

In the metathesis of **P4** with hydrosilane, a similar discussion can be presented.[41] In this reaction, not **TS4a**/**TS4b** but **Int1a**/

dx.doi.org/10.1021/ic501058j | Inorg. Chem. 2014, 53, 8485−8493

Table 1. Gibbs Activation Barrier ($\Delta G^{\circ\ddagger}$) for the Regeneration of 1 from P1 and P4 with Hydrosilane Calculated at the MP2 Level, the Stabilization Energy (ΔE_{St}) of Hypervalent Silicon Species Calculated at the MP2/6-311+G(d,p) Level, and Theoretically Predicted $\Delta G^{\circ\ddagger}$ To Complete the Catalytic Cycle[a]

	Reaction of P1 with Hydrosilane		
	$\Delta G^{\circ\ddagger}$	ΔE_{St}[b]	$\Delta G^{\circ\ddagger}$ for full catalytic cycle[c]
$HSi(OEt)_3$	4.2	−17.3	23.1
$H_2Si(OEt)_2$	11.9	−14.3	25.9
$H_3Si(OEt)$	14.8	−10.2	27.4
$HSiF_3$	~0[d]	−32.5	22.4
H_2SiF_2	6.9	−24.1	25.0
H_3SiF	10.5	−16.5	25.5
$PhSiH_3$	16.6	−2.4	30.5
	Reaction of P4 and Hydrosilane		
silane	$\Delta G^{\circ\ddagger}$	ΔG°	ΔE_{St}
$HSi(OEt)_3$	0.4	−6.5	−51.5
$PhSiH_3$	3.0	0.1	−39.4

[a]Values are presented in kcal mol^{-1}. [b]The stabilization energy in eqs 1a to 1d. [c]The energy difference between **TS1** in the second cycle and **P2** in the first cycle. [d]This value is −0.8 kcal/mol; this negative value arises from the computational procedure in which the small BS-I system was used for geometry optimization and the BS-II was employed for evaluation of energy changes.

Int1b have a hypervalent Si center. The difference in ΔE_{st} value between eqs 1c and 1d is not very different from that in ΔG° between **Int1a** and **Int1b**, as shown in Table 1, indicating that the larger hypervalency in **Int1a** is responsible for the larger exergonicity and thereby smaller activation energy of the reaction with $HSi(OEt)_3$.

Theoretical Prediction of Hydrosilane Which Can Be Applied to Hydrosilylation of CO_2. It is of considerable interest to predict theoretically what hydrosilane can be used in the hydrosilylation of CO_2. The $\Delta G^{\circ\ddagger}$ to complete the full catalytic cycle corresponds to the energy difference between **P2** of the first cycle and **TS1** in the second cycle, as was discussed above; see Figure 2. To reach **TS1** in the second cycle, we must start the reaction with **1** + $2CO_2$ + $HSiR_3$. The energy of **TS1** in the second cycle contains one molecule of $HCOOSiR_3$ because it is produced in the first cycle. The energy of **P2** in the first cycle contains those of CO_2 and $HSiR_3$ because only one CO_2 molecule is consumed when **P2** is formed from **1**. Hence,

$$\Delta G^{\circ\ddagger} = \Delta G^{\circ}(\mathbf{TS1} + HCOOSiR_3) - \Delta G^{\circ}(\mathbf{P2} + CO_2 + HSiR_3) \quad (2)$$

Because **TS1** is more unstable than **1** by 12.5 kcal/mol and **P2** is more stable than **1** by 18.2 kcal/mol in the Gibbs energy, the $\Delta G^{\circ\ddagger}$ is given below:

$$\begin{aligned}\Delta G^{\circ\ddagger} &= \Delta G^{\circ}(\mathbf{1} + 12.5 + HCOOSiR_3) - \Delta G^{\circ}(\mathbf{1} - 18.2 + CO_2 + HSiR_3)\\ &= 12.5 - (-18.2) + [\Delta G^{\circ}(HCOOSiR_3) - \Delta G^{\circ}(CO_2 + HSiR_3)]\end{aligned} \quad (3)$$

This means that the reaction energy of eq 4, the activation barrier of the CO_2 insertion, and the stability of **P2** determine the $\Delta G^{\circ\ddagger}$ of this catalytic reaction.

$$CO_2 + HSiR_3 \rightarrow HCOOSiR_3 \quad (4)$$

Hydrosilane participates only in eq 4, indicating that one can predict the dependence of $\Delta G^{\circ\ddagger}$ on hydrosilane by evaluating the reaction energy of eq 4.[42] As shown in Table 1, the reaction energy increases in the order $HSiF_3$ < $HSi(OEt)_3$ < H_2SiF_2 < H_3SiF ~ $H_2Si(OEt)_2$ < $H_3Si(OEt)$. The $\Delta G^{\circ\ddagger}$ is 25.9 kcal/mol for $H_2Si(OEt)_2$ and 25.5 kcal/mol for H_3SiF, which are not very different from the $\Delta G^{\circ\ddagger}$ (23.1 kcal/mol) of $HSi(OEt)_3$. Based on these results, we wish to present theoretical prediction that hydrosilane bearing three electronegative groups is the best and the hydrosilane bearing two to three OEt groups or one to three F groups can be applied to the hydrosilylation of CO_2; in other words, not only $HSi(OEt)_3$ but also $H_2Si(OEt)_2$, $HSiF_3$, H_2SiF_2, and H_3SiF are useful in the hydrosilylation of CO_2.

CONCLUDING REMARKS

In the hydrosilylation of CO_2, the C=O double bond of CO_2 is inserted into the Zn−H bond of **1** to afford an η^1-coordinated formate intermediate **P1** with a moderate $\Delta G^{\circ\ddagger}$ value (12.5 kcal mol^{-1}) and somewhat large exergonicity (ΔG° = −8.3 kcal mol^{-1}). **P1** isomerizes to a more stable η^2-coordinated formate complex **P2** through a very small activation barrier. Also, **1** easily reacts with methanol/water to produce [κ^3-Tptm]Zn(OMe)/[κ^3-Tptm]Zn(OH) **P4** and a dihydrogen molecule with somewhat large $\Delta G^{\circ\ddagger}$ value (17.1 kcal mol^{-1}) and somewhat large exothermicity (ΔG° = −8.1 kcal mol^{-1}). In these reactions, the CT largely occurs from the Zn−H moiety to substrate (CO_2 and MeOH) concomitantly with the polarization of the Zn−H bond.

The most interesting feature of the hydrosilylation of CO_2 is that the regeneration of **1** from **P2** significantly depends on the kind of hydrosilane. When $HSi(OEt)_3$ is used, the Si center takes a hypervalant trigonal bipyramidal structure in **TS2a**, where three OEt groups are bound with the Si atom. This geometry is favorable for the hypervalent silicon species, which is the reason for the smaller activation barrier. When $PhSiH_3$ is used, on the other hand, the activation barrier is substantially large, because the hypervalent Si species cannot be stabilized well due to the absence of an electronegative group. This is consistent with the experimental fact that $HSi(OEt)_3$ was successfully used in the CO_2 hydrosilylation but $PhSiH_3$ was not.[27]

On the contrary, the H_2 generation reaction can be performed well with $PhSiH_3$.[27] This is because the rate-determining step is the metathesis of **1** with methanol/water and the reaction of **P4** with hydrosilane easily occurs with nearly no barrier in both $HSi(OEt)_3$ and $PhSiH_3$.

It is important to propose what hydrosilane can be applied to the hydrosilylation of CO_2. The $\Delta G^{\circ\ddagger}$ value to complete the catalytic cycle depends on the energy of reaction between CO_2 and hydrosilane. Hence, the reaction energy, which we can easily calculate, provides some idea how to select hydrosilane; for instance, the hydrosilanes with two or three OEt groups or one to three F groups are expected to be useful for the catalytic hydrosilylation of CO_2.

ASSOCIATED CONTENT

Supporting Information

The optimized geometrical parameters of various important complexes, assessment of different levels of theory, the changes in Gibbs energy by CO_2 hydrosilylation, geometry changes for

dx.doi.org/10.1021/ic501058j | Inorg. Chem. 2014, 53, 8485−8493

the CO_2 insertion into Zn−H bond (pathB), the reaction of **P1** with $PhSiH_3$, the reaction of **P4** with $PhSiH_3$, and the H_2 generation reaction with water by **1**. The changes in Gibbs energy by the H_2 generation reaction with methanol. The ZPE, thermal energy, and entropy correction terms for **Int1** and **TS3**. Population changes in the CO_2 hydrosilylation reaction, the H_2 generation reaction with methanol/water, the regeneration of catalyst **1** from **P1** and silane, and that of catalyst **1** from **P4** and silane. The optimized geometry of hypervalent silicon species and the assessment of different levels of theory for stabilization energy of hypervalent species. Geometry changes in metatheses of **P1** with $H_3Si(OEt)$ and H_3SiF. Complete ref 34. This material is available free of charge via the Internet at http://pubs.acs.org.

AUTHOR INFORMATION

Corresponding Authors

*E-mail: sakaki.shigeyoshi.47e@st.kyoto-u.ac.jp.
*E-mail: milind.deshmukh@gmail.com.

Notes

The authors declare no competing financial interest.

ACKNOWLEDGMENTS

This work is financially supported by the Ministry of Education, Culture, Science, Sport and Technology through Grant-in-Aids of Specially Promoted Science and Technology (No. 22000009).

REFERENCES

(1) (a) United States Department of Energy, http://hydrogen.energy.gov/pdfs/vision_doc.pdf. (b) European Technology Platform for Hydrogen and Fuel Cells, European Commission, 2007, http://ec.europa.eu/research/fch/pdf/hfp_ip06_final_20apr2007.pdf. (c) Hydrogen and Fuel-Cell Activities in China, 2007. (d) United Nations Univ. Press, 2008, pp 295−308, http://idl-bnc.idrc.ca/dspace/bitstream/10625/35673/1/127544.pdf. (e) Stolten, D., Ed. *Hydrogen and Fuel Cells*; Wiley-VCH: 2010. (f) Muradov, N. Z.; Veziroğlu, T. N. *Int. J. Hydrogen Energy* **2008**, *33*, 6804.

(2) (a) Navarro, R. M.; Peña, M. A.; Fierro, J. L. G. *Chem. Rev.* **2007**, *107*, 3952. (b) Palo, D. R.; Dagle, R. A.; Holladay, J. D. *Chem. Rev.* **2007**, *107*, 3992. (c) Mattos, L. V.; Jacobs, G.; Davis, B. H.; Noronha, F. B. *Chem. Rev.* **2012**, *112*, 4094.

(3) For instance: Schlapbach, L.; Zuttel, A. *Nature* **2001**, *414*, 353.

(4) Eberle, U.; Felderhoff, M.; Schüth, F. *Angew. Chem., Int. Ed.* **2009**, *48*, 6608.

(5) Lim, K. L.; Kazemian, H.; Yaakob, Z.; Daud, W. R. W. *Chem. Eng. Technol.* **2010**, *33*, 213.

(6) Makowski, P.; Thomas, A.; Kuhn, P.; Goettmann, F. *Energy Environ. Sci.* **2009**, *2*, 480.

(7) For instance: (a) Staubitz, A.; Robertson, A. P. M.; Sloan, M. E.; Manners, I. *Chem. Rev.* **2010**, *110*, 4079. (b) Chen, X.; Zhao, J.-C.; Shore, S. G. *Acc. Chem. Res.* **2013**, *46*, 2666. (c) Peng, B.; Chen, J. *Energy Environ. Sci.* **2008**, *1*, 479. (d) Smythe, N. C.; Gordon, J. C. *Eur. J. Inorg. Chem.* **2010**, 509. (e) Luo, W.; Cambell, P. G.; Zakharov, L. N.; Liu, S.-Y. *J. Am. Chem. Soc.* **2011**, *133*, 19326.

(8) For instance: (a) Crabtree, R. H. *Energy Environ. Sci.* **2008**, *1*, 134. (b) Teichmann, D.; Arlt, W.; Wasserscheid, P.; Freymann, R. *Energy Environ. Sci.* **2011**, *4*, 2767. (c) Sutton, A. D.; Burrel, A. K.; Dixon, D. A.; Garner, E. B.; Gorden, J. C.; Nakagawa, T.; Ott, K. C.; Robinson, J. P.; Visilliu, M. *Science* **2011**, *331*, 1426. (d) Cambell, P. G.; Marwitz, A. J. V.; Lui, S.-Y. *Angew. Chem., Int. Ed.* **2012**, *51*, 6074.

(9) Recent reviews: (a) Johnson, T. C.; Morris, D. J.; Wills, M. *Chem. Soc. Rev.* **2010**, *39*, 81. (b) Enthaler, S.; von Langermann, J.; Schmidt, T. *Energy Environ. Sci.* **2010**, *3*, 1207. (c) Grasemann, M.; Laurenczy, G. *Energy Environ. Sci.* **2012**, *5*, 8171. (d) Centi, G.; Qudrelli, A.; Perathona, S. *Energy Environ. Sci.* **2013**, *6*, 1711. (e) Yi, N.; Saltsburg, H.; Flytzani-Stephanopoulos, M. *ChemSusChem* **2013**, *6*, 816.

(10) Recent reviews: (a) de la Piscina, P. R.; Homs, N. *Chem. Soc. Rev.* **2008**, *37*, 2459. (b) Sun, J.; Wang, Y. *ACS Catal.* **2014**, *4*, 1078.

(11) Brunel, J. M. *Int. J. Hydrogen Energy* **2010**, *35*, 3401.

(12) Luo, X. K.; Crabtree, R. H. *J. Am. Chem. Soc.* **1989**, *111*, 2527.

(13) Matarasso-Tchiroukhine, E. *J. Chem. Soc., Chem. Commun.* **1990**, 681.

(14) Schubert, U.; Lorenz, C. *Inorg. Chem.* **1997**, *36*, 1258.

(15) Chang, S.; Scharrer, E.; Brookhart, M. *J. Mol. Catal. A: Chem.* **1998**, *130*, 107.

(16) Blackwell, J. M.; Foster, K. L.; Beck, V. H.; Piers, W. E. *J. Org. Chem.* **1999**, *64*, 4887.

(17) Choi, E.; Lee, C.; Na, Y.; Chang, S. *Org. Lett.* **2002**, *4*, 2369.

(18) (a) Lee, M.; Ko, S.; Chang, S. *J. Am. Chem. Soc.* **2000**, *122*, 12011. (b) Lee, Y.; Seomoon, D.; Kim, S.; Han, H.; Chang, S.; Lee, P. H. *J. Org. Chem.* **2004**, *69*, 1741.

(19) (a) Ison, E. A.; Corbin, R. A.; Abu-Omar, M. M. *J. Am. Chem. Soc.* **2005**, *127*, 11938. (b) Corbin, R. A.; Ison, E. A.; Abu-Omar, M. M. *Dalton. Trans.* **2009**, 2850.

(20) Tan, S. T.; Kee, J. W.; Fan, W. Y. *Organometallics* **2011**, *30*, 4008.

(21) Recent reviews: (a) Jessop, P. G.; Ikariya, T.; Noyori, R. *Chem. Rev.* **1995**, *95*, 259. (b) Jessop, P. G.; Joó, F.; Tai, C.-C. *Coord. Chem. Rev.* **2004**, *248*, 2425. (c) Darensbourg, D. J. *Chem. Rev.* **2007**, *107*, 2388. (d) Sakakura, T.; Choi, J.-C.; Yasuda, H. *Chem. Rev.* **2007**, *107*, 2365. (e) Huang, K.; Sun, C.-L.; Shi, Z.-J. *Chem. Soc. Rev.* **2011**, *40*, 2435.

(22) Itagaki, S.; Yamaguchi, K.; Mizuno, N. *J. Mol. Catal. A: Chem.* **2013**, *366*, 347.

(23) (a) Motokura, K.; Kashiwame, D.; Miyaji, A.; Baba, R. *Org. Lett.* **2012**, *14*, 2642. (b) González-Sebastián, L.; Flores-Alamo, M.; García, J. J. *Organometallics* **2013**, *32*, 7186.

(24) (a) Packo, J. J.; Bailey, D. L. 1982, US 4331722. (b) Friedrich, H.; Leutner, B.; Mronga, N.; Schmid, R. 1997, EP 0778278.

(25) (a) Jansen, A.; Görls, H.; Pitter, S. *Organometallics* **2000**, *19*, 135. (b) Jansen, A.; Pitter, S. *J. Mol. Catal. A: Chem.* **2004**, *217*, 41. (c) Deglmann, P.; Ember, E.; Hofmann, P.; Pitter, S.; Walter, O. *Chem.−Eur. J.* **2007**, *13*, 2864.

(26) Lalrempuia, R.; Iglesias, M.; Polo, V.; Miguel, P. J. S.; Fernandez-Alvarez, F. J.; Perez-Torrente, J. J.; Oro, L. A. *Angew. Chem., Int. Ed.* **2012**, *51*, 12824.

(27) Sattler, W.; Parkin, G. *J. Am. Chem. Soc.* **2012**, *134*, 17462.

(28) Becke, A. D. *Phys. Rev. A* **1988**, *38*, 3098. (b) Becke, A. D. *J. Chem. Phys.* **1993**, *98*, 5648.

(29) Perdew, J. P.; Wang, Y. *Phys. Rev. B* **1992**, *45*, 13244.

(30) (a) Hehre, W. J.; Ditchfield, R.; Pople, J. A. *J. Chem. Phys.* **1972**, *56*, 2257. (b) Hariharan, P. C.; Pople, J. A. *Theor. Chim. Acta* **1973**, *28*, 213. (c) Francl, M. M.; Petro, W. J.; Hehre, W. J.; Binkley, J. S.; Gordon, M. S.; DeFrees, D. J.; Pople, J. A. *J. Chem. Phys.* **1982**, *77*, 3654.

(31) (a) Dolg, M.; Stoll, H.; Preuss, H.; Pitzer, R. M. *J. Phys. Chem.* **1993**, *97*, 5852. (b) Ehlers, A. W.; Bohme, M.; Dapprich, S.; Gobbi, A.; Hollwarth, A.; Jonas, V.; Kohler, K. F.; Stegmann, R.; Veldkamp, A.; Frenking, G. *Chem. Phys. Lett.* **1993**, *208*, 111.

(32) (a) McLean, M. D.; Chandler, G. S. *J. Chem. Phys.* **1980**, *72*, 5639. (b) Raghavachari, K.; Binkley, J. S.; Seeger, R.; Pople, J. A. *J. Chem. Phys.* **1980**, *72*, 650. (c) Frisch, J. P.; Pople, J. A.; Binkley, J. S. *J. Chem. Phys.* **1984**, *80*, 3265.

(33) Mammen, M.; Shakhnovich, E. I.; Deutch, J. M.; Whitesides, G. M. *J. Org. Chem.* **1998**, *63*, 3821.

(34) Frisch, M. J.; et al. *Gaussian 09*, revision B.01; Gaussian, Inc.: Wallingford, CT, 2010. See Supporting Information page S31 for complete reference.

(35) The reaction barrier calculated at other levels of theory shows a small negative value (∼−0.15 to −0.60 kcal mol^{-1}), indicating also that the activation barrier is negligibly small.

(36) The SCS-MP2-calculated ΔG° value is −7.4 kcal mol^{-1}, and the B3PW91 calculated one is −3.5 kcal mol^{-1}. See Supporting Information Table S3.
(37) In Figures 3 and 4, methanol dimer was taken as a starting substrate. When two independent methanol molecules were taken as starting substrates, the $\Delta G^{\circ\ddagger}$ value was 9.8 kcal/mol. This value is slightly smaller than the present $\Delta G^{\circ\ddagger}$ value (10.6 kcal/mol), but the difference is small, indicating that the evaluation of $\Delta G^{\circ\ddagger}$ with the methanol dimer as a standard is reasonable.
(38) Note that **TS5** is slightly more stable than **Int1** in the Gibbs energy but is less stable in the potential energy; see Supporting Information Table S4.
(39) (a) Sakaki, S.; Ohkubo, K. *Inorg. Chem.* **1989**, *28*, 2583. (b) Sakaki, S.; Musashi, Y. *J. Chem. Soc., Dalton Trans.* **1994**, 3047. (c) Sakaki, S.; Musashi, Y. *Inorg. Chem.* **1995**, *34*, 1914. (d) Sakaki, S.; Musashi, Y. *Int. J. Quantum Chem.* **1996**, *57*, 481. (e) Musashi, Y.; Sakaki, S. *J. Chem. Soc., Dalton Trans.* **1998**, 577. (f) Sayyed, F. B.; Tsuji, Y.; Sakaki, S. *Chem. Commun.* **2013**, *49*, 10715.
(40) We also evaluated the stabilization energy at different levels of theory; see Supporting Information page S28 for details.
(41) The geometry of **TS5a** exhibits smaller character of hypervalency than that of **TS5b**, while **TS2a** of the metathesis with $HSi(OEt)_3$ exhibits larger character of hypervalency than **TS2b** of the metathesis with $PhSiH_3$. This is not unreasonable; see page S20 in the Supporting Information for details.
(42) This discussion can be presented when **TS2** does not become higher in energy than **TS1** in the second cycle. In the metatheses of **P1** with $H_2Si(OEt)_2$, $H_3Si(OEt)$, H_2SiF_2, and H_3SiF, the $\Delta G^{\circ\ddagger}$ values relative to **P1** are 11.9, 14.8, 6.9, and 10.5 kcal/mol, respectively; see Figure S11 in the Supporting Information for geometry of transition state. These values show that the ΔG° values of **TS2** are 3.9, 6.5, 1.4, and 2.2 kcal/mol for $H_3Si(OEt)$ and H_3SiF, respectively. These are smaller than those of **TS1** in the second cycle, which are 7.7, 9.2, 6.8, and 7.3 kcal/mol for $H_2Si(OEt)_2$, $H_3Si(OEt)$, H_2SiF_2, and H_3SiF, respectively. Hence, the $\Delta G^{\circ\ddagger}$ to complete the catalytic cycle is the energy difference between **P2** in the first cycle and **TS1** in the second cycle in these hydrosilanes.

■ NOTE ADDED AFTER ASAP PUBLICATION

This paper was published on the Web on July 30, 2014, with minor errors in Figure 3. The corrected version was reposted on July 31, 2014.